Journal of Applied Statistics, 2013
Vol. 40, No. 6, 1270–1288, http://dx.doi.org/10.1080/02664763.2013.785492

Taylor & Francis
Taylor & Francis Group

Segmentation, alignment and statistical analysis of biosignals with application to disease classification

Sebastian Kurtek[a]*, Wei Wu[b], Gary E. Christensen[c] and Anuj Srivastava[b]

[a]*Department of Statistics, The Ohio State University, Columbus, OH, USA;* [b]*Department of Statistics, Florida State University, Tallahassee, FL, USA;* [c]*Electrical and Computer Engineering, University of Iowa, Iowa City, IA, USA*

(*Received 2 February 2012; accepted 11 March 2013*)

We present a novel methodology for a comprehensive statistical analysis of approximately periodic biosignal data. There are two main challenges in such analysis: (1) the automatic extraction (segmentation) of cycles from long, cyclostationary biosignals and (2) the subsequent statistical analysis, which in many cases involves the separation of temporal and amplitude variabilities. The proposed framework provides a principled approach for statistical analysis of such signals, which in turn allows for an efficient cycle segmentation algorithm. This is achieved using a convenient representation of functions called the square-root velocity function (SRVF). The segmented cycles, represented by SRVFs, are temporally aligned using the notion of the Karcher mean, which in turn allows for more efficient statistical summaries of signals. We show the strengths of this method through various disease classification experiments. In the case of myocardial infarction detection and localization, we show that our method compares favorably to methods described in the current literature.

Keywords: functional data analysis; cyclostationary biosignal segmentation; myocardial infarction; gait; disease classification

1. Introduction

Computer intervention in medicine provides many advantages ranging from automatic and quantitative analysis to removal of subjective variation in diagnosis across physicians. In many medical applications, the quantities used for disease diagnosis and monitoring are functions of time such as blood pressure or electrocardiogram (ECG) signals. However, due to large subject variability in the studies, the time domains of these measurements are not the same. This random temporal variability, if not accounted for, can cloud the statistical analysis. Furthermore, many of the functions of interest are approximately periodic and sampled at a very high resolution. A direct analysis of these long biosignals is often computationally inefficient and prone to being affected

*Corresponding author. Email: kurtek.1@stat.osu.edu

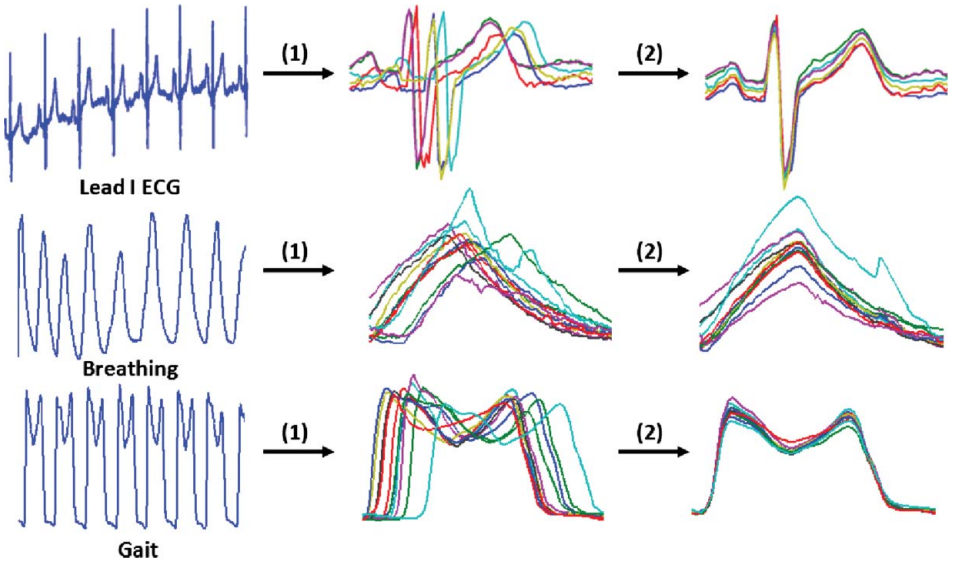

Figure 1. Analysis of biomedical signals involves automatic cycle segmentation and temporal alignment. *Left*: Long approximately periodic signal. *Middle*: Cycles segmented from the long biosignal. Note that these are not temporally aligned. *Right*: Segmented cycles after additional temporal alignment. Note the improved correspondence of features in the signals.

by noise. Thus, a common approach is to summarize such biosignals using cross-sectional statistics such as the mean, median and variance, and then use standard statistical tests as diagnostic tools. This type of analysis ignores the underlying temporal variability of the data, and as a result, can provide unreliable and biased conclusions. If, on the other hand, it was possible to segment the long cyclic signals into their corresponding cycles and to form a template cycle (averaging out the noise), this template could be used for further analysis. Thus, the main challenges faced in analysis of periodic biomedical signals are: (1) automatic extraction of cycles from long temporal biosignals and (2) automatic temporal alignment of the cycles in a principled manner. We present the motivation for this work using three real examples shown in Figure 1. In many applications, the raw data come in the form of a long periodic biosignal as displayed in the left panel. We are interested in first extracting the cycles from this signal in an automated manner. The extracted cycles are displayed in the middle panel. After extraction, there is no guarantee that the cycles are in optimal temporal correspondence. This can also be seen in the middle panel in the figure where the features of the signal cycles do not match very well. Thus, we are left with the task of performing an additional temporal alignment, which provides a separation of phase and amplitude variabilities in the signal cycles. The aligned cycles are displayed in the right panel where it can be seen that the only variability remaining is amplitude. It is important to note that the required alignment is not always a linear shift and thus non-linear time warping is required.

1.1 *Biosignals as diagnostic tools*

Measurement, imaging, analysis and characterization of normal and abnormal pulmonary function and anatomy are often limited by our ability to accurately and robustly identify the beginning and end of each respiratory cycle. Further complicating matters are temporal distortion of the breathing cycle due to breathing variation from one breath to the next. Breathing variation is caused by changes in breathing effort, the volume of inhaled air, abdominal vs. thoracic breathing and disease. Therefore, it is important to be able to identify corresponding time points from one breathing cycle

to the next especially in the case of free breathing. For example, improving the reproducibly and identification of consistent breathing cycle time points has the potential to improve 4D computed tomography (CT) and positron emission tomography (PET) image reconstruction. 4D imaging of the lung often requires data to be acquired over multiple breathing cycles and binned into similar breathing phases. A common reconstruction approach is to reconstruct a certain number of 3D image volumes (for example 10) based on the phase of the breathing cycle. Data is grouped together from multiple breathing cycles to reconstruct each 3D image volume. The phases are defined by break points during the breathing cycle and are usually not equally spaced over the breathing cycle. Using the proposed method (PM) may improve the accuracy and repeatability of selecting these breaks and thereby improve image quality and the subsequent image processing analysis of these data. Another potential application of the method is improved prediction of the state of the lung during radiotherapy of lung cancer. The goal of radiotherapy of lung cancer is to maximize the radiation dose delivered to the tumor while reducing the dose given to healthy tissue. Breath-hold, gating and trained breathing based on auditory cues are common methods for minimizing breathing variation during radiotherapy. However, patients with lung disease often have trouble holding their breath and trained breathing does not guarantee reproducible breathing. Radiation gating refers to the technique of turning on and off the radiation source when the tumor comes in and out of a particular phase of the breathing cycle. The PM has the potential to improve radiation gating by more accurately identifying lung position/motion in real time and possibly eliminate gating entirely if the position/motion of the lung is known.

Neuro-degenerative diseases often affect gait and mobility. In particular, Huntington's and Parkinson's diseases affect the striatum (caudate and putamen) in the basal ganglia, which among other things is responsible for motor control [14]. This condition impairs a subject's ability to maintain a steady walk with small stride-to-stride fluctuations. The third neuro-degenerative disorder that we consider in this paper is amyotrophic lateral sclerosis, which affects the motoneurons of the cerebral cortex, brain stem and spinal cord. In this disease, it is unknown whether the stability and stride-to-stride dynamics of gait are affected [13]. The ability to assess gait differences between control and disease groups could provide a useful and inexpensive diagnostic tool and possible insights into disease progression.

Myocardial infarction (MI) is the leading cause of morbidity and mortality in the world [1]. The American Heart Association defines MI as the damaging or death of an area of the heart muscle (myocardium) resulting from a blocked blood supply (ischemia) to that area [1]. The recording of fluctuations in electrical potential of the heart muscle on the body surface is called the ECG. A vector that represents the magnitude and direction of the electric field generated through the heart is called a cardiac vector [5]. In the ECG, the amplitude recorded on a given lead depends on the projection of the cardiac vector on that lead at that time. Hypertrophic and atrophic structural changes as well as electrical conduction of the heart are frequently associated with a reduced blood supply to the heart. These changes affect the magnitude and direction of the normal cardiac vector causing alterations in the amplitude and morphology of ECG waves in different leads [5]. The ECG is a widely used and cheap diagnostic tool used to investigate and diagnose MI. Thus, automated algorithms that can accurately and efficiently analyze ECG signals can be useful in monitoring and identifying the risk or onset of the disease. In addition, it would be very useful to identify the area of the heart, which becomes ischemic. In this work, we address both of these goals.

1.2 *Statistical functional data analysis*

Statistical analysis of cyclostationary biosignals falls under a larger category of statistical functional data analysis. There exists a large literature on statistical analysis of functions, in part due to the pioneering efforts of Ramsay and Silverman [25], Kneip and Gasser [16], and several others [20,27]. When restricting to the analysis of elastic functions (functions that are temporally

aligned) the literature is relatively recent and limited [8,15,17,20,24,27]. There are basically two categories of the past papers on this subject. One set treats the problem of temporal alignment as a pre-processing step. Once the functions are aligned, they are analyzed using standard tools from functional data analysis, e.g. the cross-sectional mean, covariance computation and functional PCA. The second set of papers study both comparison (includes temporal alignment) and analysis jointly, using energy-minimization procedures. Although the latter generally provides better results due to a joint solution, the choice of the energy function used to provide this solution is problematic, which we explain next.

We introduce some additional notation. We will consider biosignals as real-valued functions on $[0, 1]$. Let Γ be the set of orientation-preserving diffeomorphisms of the unit interval $[0, 1]$: $\Gamma = \{\gamma : [0, 1] \to [0, 1] | \gamma(0) = 0, \gamma(1) = 1, \gamma \text{ is a diffeomorphism}\}$. For a function $f \in \mathcal{F}$, where $\mathcal{F}$ is an appropriate space of functions on $[0, 1]$ (defined later), the composition $f \circ \gamma$ denotes temporal warping of f using γ. A majority of past methods study the problem of alignment and comparison of functions, either separately or jointly, by solving $\inf_{\gamma \in \Gamma} \|f_1 - (f_2 \circ \gamma)\|$. The use of this quantity is problematic because it is not symmetric and can lead to degenerate results. The optimal alignment of f_1 to f_2 gives a different minimum, in general, when compared with the optimal alignment of f_2 to f_1. As a result, this formulation does not lead to a proper distance between the registered functions which is important for computing meaningful statistical summaries such as the mean, covariance and principal component analysis.

To support these claims, we present a simple set of functional data alignment results generated by several different methods in current literature and compare these results to the method proposed in this paper, which does not have the issues stated above. We present these results for three different types of biosignals (ECG PQRST complexes, gait and respiration cycles) in Figure 2. We note that the PM outperforms all of the other methods with respect to the quality of the alignment of the biosignals. The other methods are mainly parametric or moment-based. For real data that cannot be well described by a parsimonious parametric representation or low-order moments, these methods may miss main structures in the data and result in unfavorable performance in alignment as is seen in the provided examples. In contrast, our method is fully nonparametric, and in general can deal with any (absolutely continuous) functions. Additionally, many of the other methods destroy the structure of the original biosignals, which is a highly undesirable effect, especially when performing statistical analysis of biological data.

1.3 *Proposed method*

In this work we propose a novel technique for segmentation and subsequent analysis of biosignals with application to disease detection. This framework, which was previously introduced in [18,26] is based on elastic functional data analysis, where the function comparison and alignment is simultaneous. The main difference between this framework and the ones mentioned in the previous section is that the registration and comparison of functions are performed under the same metric. Furthermore, a careful selection of this metric allows us to define proper distances between time-warped functions, and to compute intuitively meaningful sample statistics.

As an overview, our approach to analyze long biosignals works as follows:

(1) Segment the biosignal into its cycles (if it is cyclostationary). Cycle extraction is an important problem in analysis of biosignal data. As an example, each lead signal in the ECG data presented in this paper contains a 10 s interval with 1000 measurements per second. Using the full signal for analysis is thus computationally expensive and inefficient in disease classification studies.
(2) Based on the extracted cycles, form a signature complex (using the sample mean of cycles) for each subject in the study. In more general terms, we provide a setting for comprehensive

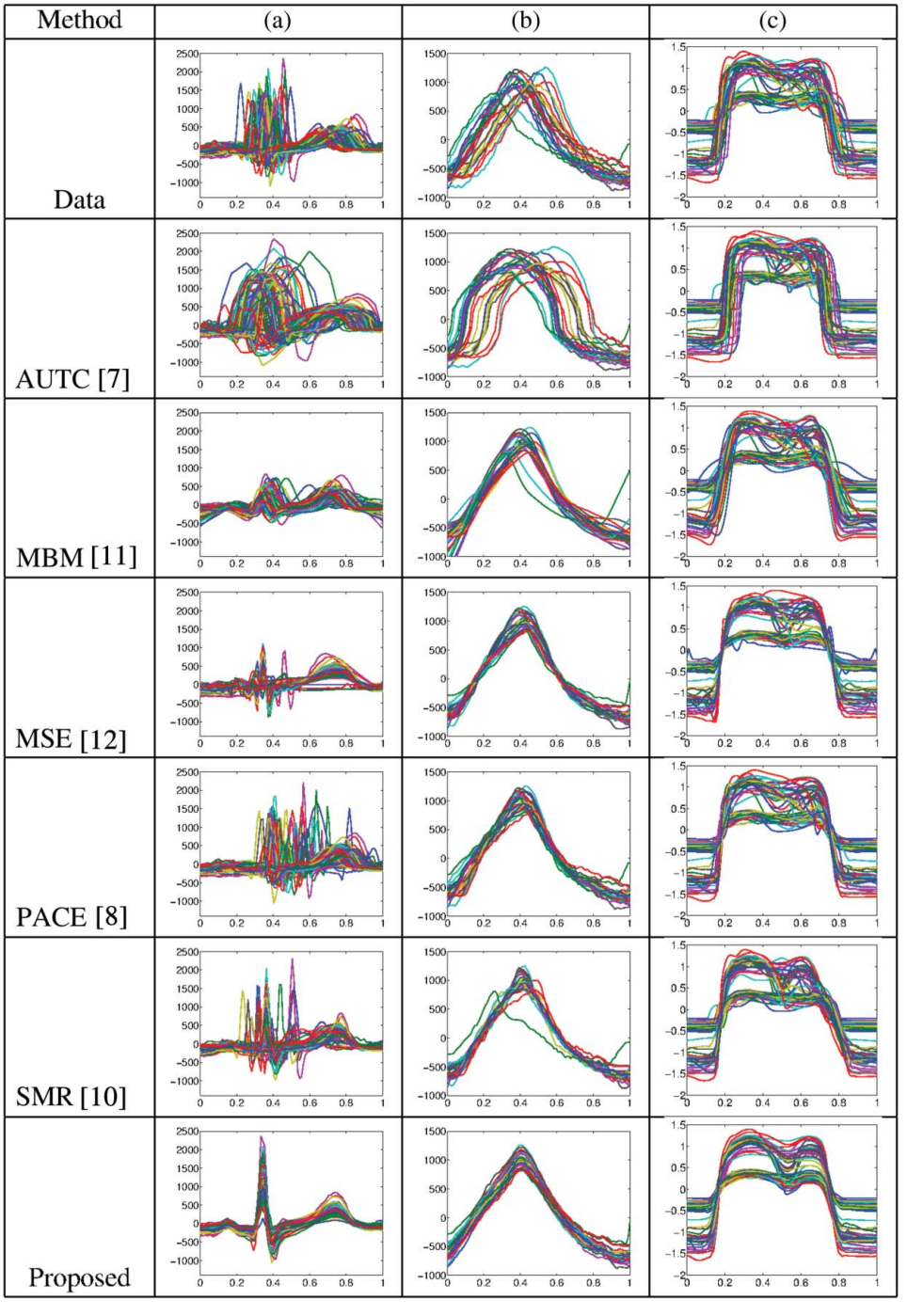

Figure 2. Comparison of temporal alignment quality based on different methods in the literature. The alignment was performed on different types of biosignals including (a) ECG data, (b) gait data and (c) respiration data.

statistical analysis of biosignals, where one is able to compute the sample mean, covariance and perform dimension reduction using principal component analysis.

(3) Perform classification using all pair-wise distances between signature complexes of all subjects.

As will be made clear later, the entire process is fully automatic. This approach is different from the majority of previous methods as it does not rely on selecting and computing features from the extracted cycles [6,22].

The rest of this paper is organized as follows. In Section 2, we present the methodology for elastic functional data analysis of biosignals. In this section, we also outline an automatic segmentation algorithm for cyclostationary biosignals. In Section 3, we consider two disease detection problems. First, we focus on detection of amyotrophic lateral sclerosis, Parkinson's and Huntington's diseases based on gait data. Second, we consider the tasks of detecting and localizing MI using ECG signals.

2. Methods

In this section, we introduce the data sets used for analysis and the general framework for elastic functional data analysis.

2.1 *Data description*

There are three data sets used in this paper.

Respiration data: Here, Siemens BIOGRAPH 40 software was used to sort raw 4D-CT images into respiratory phase-based bins of 4D-CT images. The Anzai strain gauge belt utilizes a pressure sensor to measure changes in strain during respiration. The amplitude of the strain signal is adjusted for each data point relative to the maximum and minimum inflection points for each cycle of respiration. The system then calculates a relative amplitude-based phase at each point of a respiratory trace, where 0% corresponds to end expiration and 100% corresponds to peak inspiration. In this application, we will focus on the problem of segmenting the long strain respiration signal into respiration cycles. This provides an automatic framework for detection of change points, which allows easy identification of corresponding measurements of interest (such as full CT images). An example of a cyclostationary respiration biosignal is displayed in Figure 3(a).

Gait data: This data came from the gait dynamics in neuro-degenerative disease database, which was obtained from Physionet [11]. The records in this database came from four types of subjects: 15 with Parkinson's disease, 19 with Huntington's disease, 12 with amyotrophic lateral sclerosis and 16 controls. The raw data were obtained using force-sensitive resistors, with the

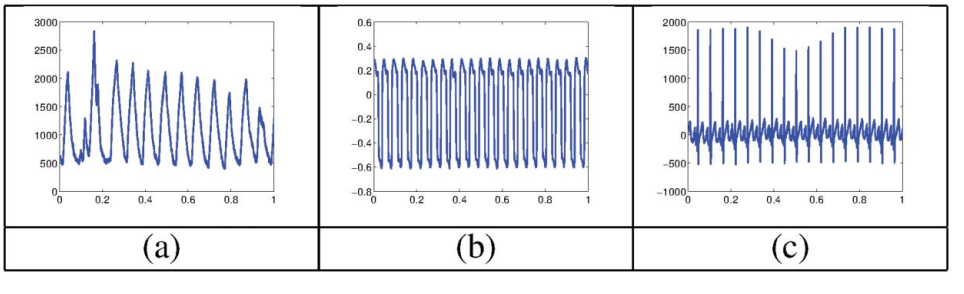

Figure 3. Examples of long cyclostationary biosignals coming from (a) respiration data, (b) gait data and (c) ECG data.

output roughly proportional to the force under the foot. Seven stride-to-stride measures of footfall contact times (also functions of time) were derived from these signals: (1) left stride interval (s), (2) right stride interval (s), (3) left swing interval (s), (4) right swing interval (s), (5) left stance interval (s), (6) right stance interval (s) and (7) double support interval (s). We utilized the raw 'force under the foot' data (cyclic) to showcase our temporal segmentation algorithm, and the stride-to-stride measures for disease detection. As suggested in [13,14], we filtered the stride-to-stride measure data by removing outliers outside three standard deviations around the median. An example of a cyclostationary gait biosignal is displayed in Figure 3(b).

ECG data: This data is a subset of the Physikalisch-Technische Bundesanstalt (PTB) diagnostic ECG database [3], which was also obtained from Physionet [11]. It consists of 80 healthy control ECGs (28 are repeated measures for the same subject) and 80 MI ECGs (no repeated measures). The data provided for each subject are the 12 standard ECG lead signals as well as the three Frank ECG leads VX, VY and VZ. In addition, in case of MI, a detailed diagnosis and localization of the infarction are provided. Each ECG channel had synchronous 1 kHz sampling frequency and we used a 10 s interval for each subject in the analysis. An example of a cyclostationary ECG biosignal is displayed in Figure 3(c).

2.2 *Representation space of biosignals*

Now, we present our framework. As a first step, we seek representations and metrics that can compare and temporally align functions simultaneously. Let f be a real-valued function (ECG signal, respiration cycle, etc.) with the domain $[0, 1]$. Let $\mathcal{F}$ denote the set of all such functions. Also, let Γ be the set of orientation-preserving diffeomorphisms of the unit interval $[0, 1]$. Elements of Γ are used to represent temporal warping of functions. One would like a principled framework to compare elements of $\mathcal{F}$ and to compute statistics on $\mathcal{F}$. The problem with the common approach is that $\|f_1 - f_2\| \neq \|f_1 \circ \gamma - f_2 \circ \gamma\|$ and therefore it is not possible to define a mean of functions with warping variability, because of the lack of a proper distance (satisfies the triangle inequality, is non-negative and symmetric).

We seek a distance on $\mathcal{F}$ such that $d(f_1, f_2) = d(f_1 \circ \gamma, f_2 \circ \gamma)$. In fact, there exists such a distance called the Fisher–Rao distance. This metric has many fundamental advantages, including the fact that it is invariant to domain warping [4]. Unfortunately, this distance is difficult to compute because the metric changes from point-to-point on the space of functions. To solve this issue we have defined a function q, which we refer to as the square-root velocity function or SRVF, as $q : [0, 1] \to \mathbb{R}$, where $q(t) = \text{sign}(\dot{f}(t))\sqrt{|\dot{f}(t)|}$. It can be shown that if the function f is absolutely continuous, then the resulting SRVF is square-integrable. Furthermore, if we temporally warp a function f by γ, the SRVF of $f \circ \gamma$ is given by $\tilde{q}(t) = (q, \gamma) = (q \circ \gamma)(t)\sqrt{\dot{\gamma}(t)}$. The SRVF representation has been previously introduced in [18,26]. The main motivation for using the SRVF for functional data analysis is that under this representation, the complicated Fisher–Rao metric becomes the standard $\mathbb{L}^2$ metric. This result can be used to compute the distance d_{FR} between any two functions as follows. Simply compute the $\mathbb{L}^2$ distance between the corresponding SRVFs and set d_{FR} equal to that value: $d_{\text{FR}}(f_1, f_2) = \|q_1 - q_2\|$. We define $\mathcal{C} = \mathbb{L}^2([0, 1], \mathbb{R})$ to be the set of all SRVFs. For every $q \in \mathcal{C}$ there exists a function f (unique up to a constant, or a vertical translation) such that the given q is the SRVF of that f. In fact, this function can be obtained precisely using the equation: $f(t) = f(0) + \int_0^t q(s)|q(s)|\text{ds}$. Thus, the representation $f \Leftrightarrow (f(0), q)$ is invertible. Note that because we use SRVFs (defined using the derivative of the biosignal) to analyze biosignals, the baseline (or vertical) variability is automatically removed. In many biomedical applications (such as analysis of ECG signals) this is a desired effect. Nonetheless, as will be seen in the gait example in a later section, there are diseases that only mainly affect the baseline variability. In those cases, our method may have trouble differentiating the control and disease groups.

2.3 *Pair-wise function alignment*

So far we have defined the Fisher–Rao distance on $\mathcal{F}$ and have found a simple way to compute it using SRVFs. But, we have not involved any temporal alignment in the distance calculation and thus it represents a non-elastic comparison of functions. The next step is to define an elastic comparison of functions using equivalence classes of SRVFs under the action of Γ. The equivalence class of an SRVF $q \in \mathcal{C}$ under this action is given by: $[q] = \text{closure}\{(q, \gamma)|\gamma \in \Gamma\}$. It is the set of SRVFs associated with all the time warpings of a given function. Any two functions in the set $[q]$ differ only in their temporal alignment. Let $\mathcal{S}$ denote the set of all such equivalence classes. To compare any two equivalence classes we will use the metric imposed on $\mathcal{C}$. This metric leads to a definition of geodesic distances on $\mathcal{S}$.

DEFINITION 2.1 *For any two functions $f_1, f_2 \in \mathcal{F}$ and the corresponding SRVFs, $q_1, q_2 \in \mathcal{C}$, we define the distance d to be:* $d([q_1], [q_2]) = \inf_{\gamma\in\Gamma} \|q_1 - (q_2 \circ \gamma)\sqrt{\dot{\gamma}}\|$.

The minimizer of d will be denoted by γ^* and $(q_2 \circ \gamma^*)\sqrt{\dot{\gamma}^*}$ by q_2^*. In this process, one performs function alignment using the minimization step. Note that the distance d between a function and any domain-warped version of the same function is zero. However, it can be shown that if the SRVFs belong to different equivalence classes, then the distance between them is strictly positive. Thus, the distance d is a proper distance on $\mathcal{S}$. Furthermore, we can compute the geodesic path (optimal deformation) between two functions using a linear interpolation between their SRVFs (for $\tau \in [0, 1]$): $\eta(\tau) = \tau q_2^* + (1 - \tau)q_1$.

In Figure 4, we present three results of computing linear interpolation paths between SRVFs of different types of biosignals. Note that we display the biosignals themselves and not the SRVFs. In the first example, we consider comparing two respiration cycles. In the second example, we compare two left foot pressure signals coming from gait analysis, and in the last example we show a path between two PQRST complexes coming from ECG signals. We compare the resulting linear interpolation paths in $\mathcal{C}$ (panel (b), no temporal alignment) and $\mathcal{S}$ (panel (c), temporally aligned). In panel (a) of each example, we show f_1 (first signal in blue), f_2 (second signal in red) and $f_2 \circ \gamma^*$ (aligned second signal in green). Finally, we also display γ^* in panel (d). We display these paths by showing seven functions sampled at equal distances along the path. It is easy to see that the optimization over Γ provides a much nicer alignment of the biosignals. This in turn provides more accurate measures of differences between them and more natural linear interpolations between SRVFs, which results in nicely preserved features of the biosignals. To make this more precise, let us consider the ECG example. The path (panel (b)) between the two biosignal cycles with their given temporal alignment does not preserve their natural features such as the distinct PQRST points (correspond to the first positive wave, the first negative wave, the sharp second positive wave, the second negative wave and the final positive wave, respectively). The proposed framework allows us to compute the optimal temporal alignment between the two cycles. The resulting path (panel (c)) preserves the previously mentioned features. That is, any signal cycle on the interior of this path also contains distinct PQRST points. Because we allow for this non-linear alignment, we are not restricted to the given alignment of the biosignals. The deviations in the placement of the functions on our time domain are removed by aligning them optimally according to our distance measure d. This appears to be very important in many medical applications due to very high variability across subjects. Clearly, different people breathe at different rates and have very different heart rates resulting in altered ECG signals. Thus, in order to obtain an accurate comparison of such biosignals coming from two different subjects, they must first be placed on the same time domain, which can be achieved through temporal alignment.

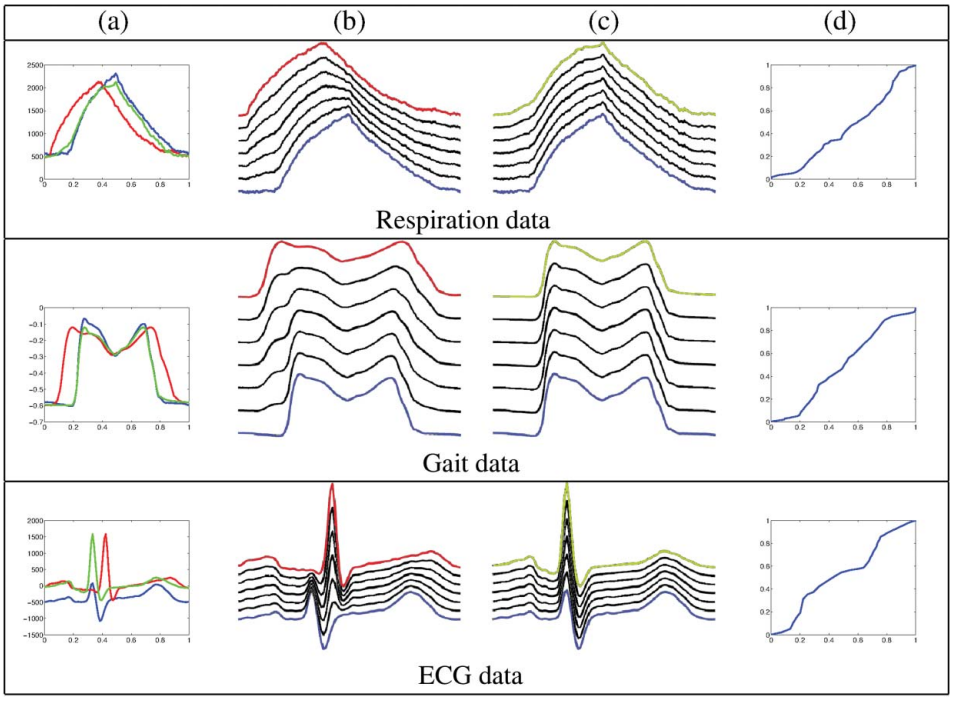

Figure 4. Examples of geodesics between biosignals (linear interpolations between SRVFs). (a) Two given biosignal cycles (blue and red) and the red biosignal cycle after temporal alignment (green). (b) Curves showing the intermediate biosignals of the blue biosignal as it evolves into the red biosignal along the path. (c) Same as (b) except the curves were sampled along the path from the blue biosignal to the green biosignal (i.e. red biosignal aligned to blue). The curves have been separated vertically for visualization purposes. (d) The function that optimally aligns the red biosignal to the blue biosignal (denoted by γ^*). Note that the curves between the biosignals presented here were sampled at seven equally spaced time points along the path.

2.4 *Karcher mean and multiple function alignment*

An important goal of this framework is to align multiple functions horizontally to improve the matching of features across biosignals. This is accomplished naturally using the notion of the Karcher mean. First we define and compute a mean function in $\mathcal{S}$ and during that process we temporally align the SRVFs of the given functions to match the mean function.

For a given collection of functions $f_1, f_2, \ldots, f_n$, let $q_1, q_2, \ldots, q_n$ denote their SRVFs, respectively. A notion of a mean of these functions is defined as follows.

DEFINITION 2.2 *Define the Karcher mean of the given SRVFs as a local minimum of the cost function*:

$$[\hat{\mu}] = \underset{[q]\in\mathcal{S}}{\operatorname{argmin}} \sum_{i=1}^{n} d([q],[q_i])^2. \tag{1}$$

We emphasize that the Karcher mean is actually an equivalence class $[\hat{\mu}]$ of functions, rather than being an individual function. However, for the purpose of plotting a mean function and for subsequent analysis involving the mean, it is desirable to have an element of $[\hat{\mu}]$ that best represents the temporal variability of the original data. In our method, there is a very natural choice of this element. We choose the element of $[\hat{\mu}]$, which ensures that the mean of $\{\gamma_i^*\}$, denoted by $\gamma_{\hat{\mu}}$, is

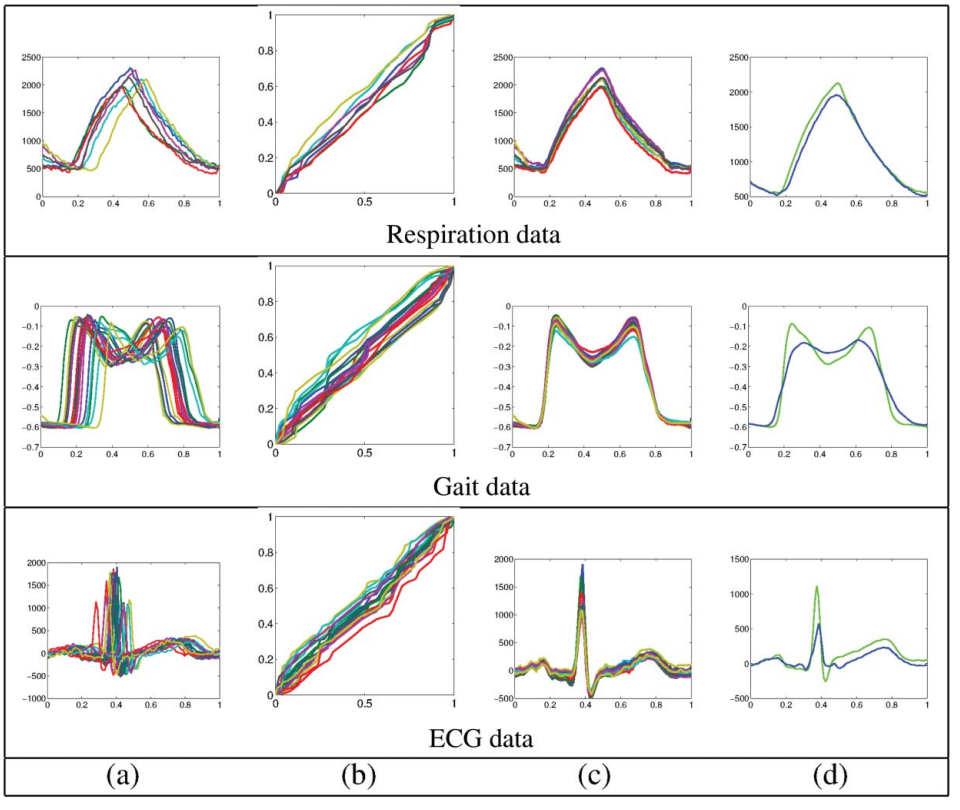

Figure 5. Karcher mean computation of different types of biosignals (top: respiration; middle: gait; bottom: ECG). (a) Original biosignals, (b) warping functions, (c) warped biosignals and (d) comparison of means before temporal alignment (blue, also called the point-wise mean) and after temporal alignment (green).

$\gamma_{id}(t) = t$. The selection of this preferred element of $[\hat{\mu}]$ is performed as the final step in the mean computation algorithm. The full algorithm for computing the Karcher mean of SRVFs is given in previous papers [18,26]. This procedure results in three items: (i) $\hat{\mu}$, preferred element of the Karcher mean equivalence class $[\hat{\mu}]$, (ii) $\{\tilde{q}_i\}$, the set of aligned SRVFs, and (iii) $\{\gamma_i^*\}$, the set of optimal alignment functions with mean γ_{id}.

In Figure 5, we present examples of computing mean biosignals for the three applications of interest (respiration, gait and ECG data). In each example, we display the original set of biosignals without warping, the computed warping functions γ_i^*, the aligned biosignals and a comparison of two means, the cross-sectional (point-wise) mean without temporal alignment (blue) and the Karcher mean in $\mathcal{S}$ (green). Again, we see that the features of the Karcher mean are nicely preserved due to crisp temporal alignment of the given functions.

2.5 *Temporal segmentation of cyclic biosignals*

So far we have studied the biosignals using optimal alignments of their time domain. However, we will utilize the temporal alignment functions (γ^*) to specify a fully automatic algorithm for segmentation of approximately cyclostationary signals. First, we introduce a framework for quantifying differences between temporal warping functions and then we will focus on the segmentation algorithm.

Our goal is to develop a distance function that can measure the amount of temporal alignment needed to optimally align two biosignals. Thus, we are faced with defining a metric on the

space of temporal alignment functions and computing geodesic distances under this metric. This process is greatly simplified using a convenient transformation, which coincidentally is similar to the definition of the SRVF. We are going to represent an element $\gamma \in \Gamma$ by the square-root of its derivative $\psi = \sqrt{\dot{\gamma}}$. Note that this is the same as the SRVF defined earlier for f_is and takes this form since $\dot{\gamma} > 0$. The identity map γ_{id} maps to a constant function with value $\psi_{id}(t) = 1$. An important advantage of this transformation is that since $\|\psi\|^2 = \int_0^1 \psi(t)^2 \mathrm{d}t = \int_0^1 \dot{\gamma}(t)\mathrm{d}t = \gamma(1) - \gamma(0) = 1$, the set of all such ψs is the positive orthant of the unit sphere in $\mathbb{L}^2$. The Fisher–Rao distance between any two temporal alignment functions is the arc-length between the corresponding SRVFs $d_{\mathrm{FR}}(\gamma_1, \gamma_2) = d_\psi(\psi_1, \psi_2) \equiv \cos^{-1}(\int_0^1 \psi_1(t)\psi_2(t)\mathrm{d}t)$. In order to quantify the amount of temporal alignment needed to match two biosignals, we use the distance $d_{\mathrm{FR}}(\gamma_{id}, \gamma^*)$. That is, we use the identity function for the first biosignal cycle (we do not temporally warp this function) and γ^* for the second cycle which is the function that temporally aligns the second cycle to the first one in an optimal manner.

Now, we focus on applying the analysis of alignment functions to an automatic segmentation algorithm of periodic biosignals. Given a long biosignal and a cycle template, we will automatically extract multiple cycles from that signal. A pictorial depiction of the main idea is shown in Figure 6 using ECG signal data. We perform this segmentation as follows. We initialize with the template starting at the beginning of the given signal. The template can either be chosen as one cycle in the signal or the Karcher mean of multiple cycles (chosen manually). At each iteration, we slide the template along the signal and compute the amount of temporal alignment needed (d_ψ) to align the template to the overlapping segment of the signal. The sliding step and overlap window parameters depend on the application of interest. Note that this is considerably different from a sliding window approach that utilizes the $\mathbb{L}^2$ distance. In our approach we do not use the amplitude information of the biosignals. Instead, we quantify (using d_ψ) the amount of temporal alignment needed to match the template to the signal in the current window. If this distance is small then the template and the signal in the current window correspond to each other very well and the signal in the window is extracted as one of the cycles. Because the cycles are repeated throughout the signal, the resulting distance function is harmonic and the minima of this function represent the segments of interest, i.e. the segmented cycles. We also have a refinement step, which considers inclusion or exclusion of a small neighborhood around the starting and ending points. Once extracted, there is no guarantee that the cycles are temporally aligned and thus we

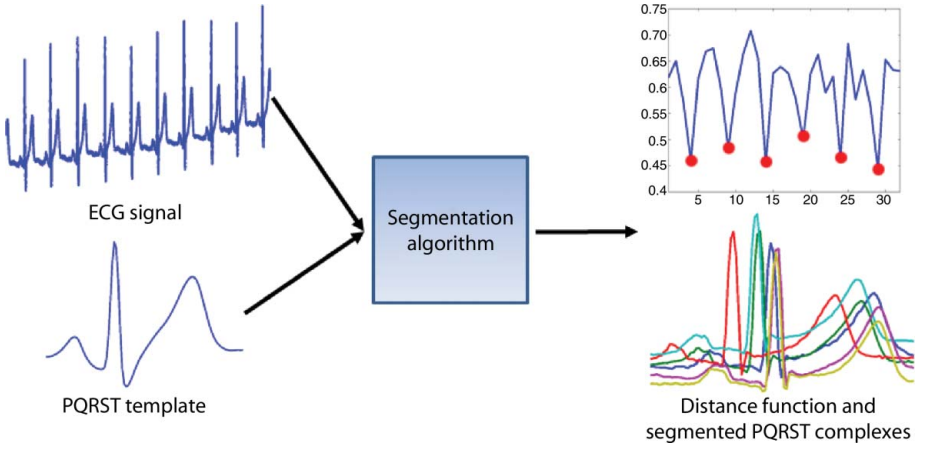

Figure 6. Segmentation algorithm. The inputs are a long periodic biosignal and a template. The output consists of the extracted cycles, which correspond to the minima (marked with red dots) of the d_ψ function, which is harmonic.

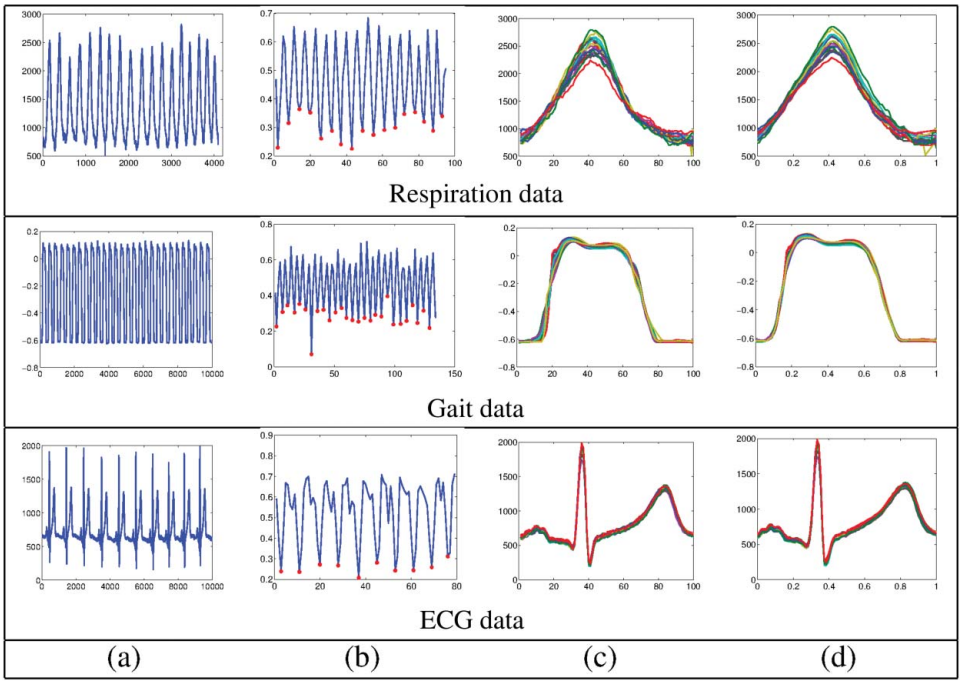

Figure 7. (a) Long cyclic signal. (b) Harmonic cost function based on d_ψ. (c) Cycles segmented from the biosignals. (d) Cycles after additional temporal alignment.

use the Karcher mean for this purpose. We have applied this segmentation algorithm to the three data sets described earlier. A segmentation result for each of the different data sets is presented in Figure 7. Note that the red dots marking the minima of the cost function correspond to the extracted cycles.

An important property of this segmentation algorithm is that it is robust to the amplitude scale of the cycles. This is due to the fact that the cost function used in our algorithm depends only on the distance between temporal alignment functions. As mentioned earlier, this distance is independent of the difference in amplitude of the template cycle and the cycles we want to segment. We can compare our method to one that uses the $\mathbb{L}^2$ distance between signal fragments to segment the cycles. To do this, we generated an artificial periodic signal using Gaussian kernels with two different amplitude scales. As a template, we chose a cycle (single Gaussian bump) with the smaller amplitude. The segmentation results are presented in Figure 8. It is clear that the distance we use in our segmentation algorithm provides a much better structure in the cost function used to segment the periodic signal. When the $\mathbb{L}^2$ distance is used, it is very hard to identify all of the minima in the cost function. Thus, this method does not provide a good segmentation of the signal where both higher and lower amplitude cycles are identified. In fact, it is only able to segment the cycles with the lower amplitude, which corresponds to the amplitude of the template.

3. Application to disease classification

In this section, we present two types of results. First, we give disease detection results based on stride-to-stride gait measurements. Second, we give results on MI detection and localization based on ECG biosignal data.

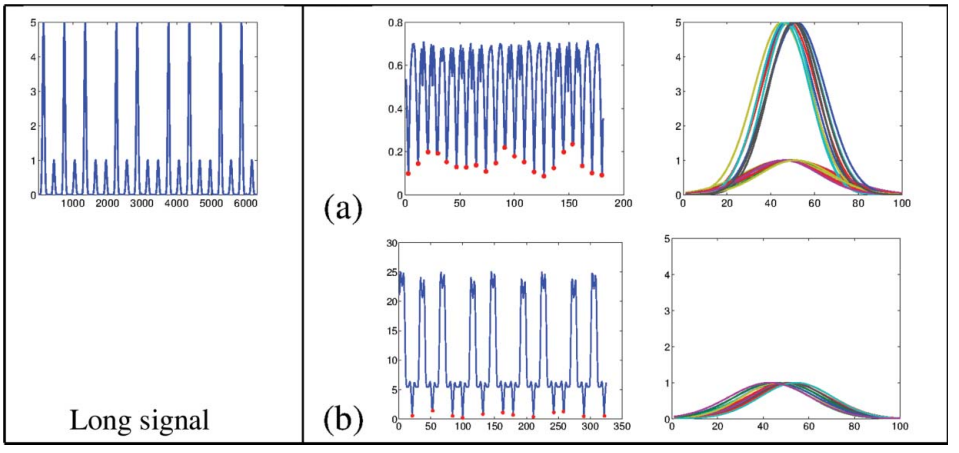

Figure 8. Artificial example of segmenting a long periodic signal, which contains cycles with drastically different amplitudes. (a) PM. (b) Method based on $\mathbb{L}^2$ cost function.

3.1 *Disease classification using stride-to-stride gait data*

In this section, we will utilize stride-to-stride gait data described in Section 2.1. There are four different groups in this data set (amyotrophic lateral sclerosis or ALS, Huntington's disease, Parkinson's disease and controls). We will consider stride-to-stride measures for disease classification purposes. We are interested in using the proposed distance (d, utilizes temporal alignment, defined in Section 2.3) between each pair of such measures to differentiate between each of the disease groups and the control group. We compare our result to a simple $\mathbb{L}^2$ distance between the stride-to-stride measures without temporal alignment. In all of these classification studies, we use the leave-one-out nearest neighbor classifier (LOO-NN). We report the accuracy ($\text{AC} = (\text{TP} + \text{TN})/(\text{TP} + \text{TN} + \text{FP} + \text{FN})$) for each of the diseases separately, where TP and FP are the numbers of true and false positives, respectively, and TN and FN are the numbers of true and false negatives, respectively. The results are presented in Table 1, where we mark the best performance in bold. The proposed distance d clearly outperforms the $\mathbb{L}^2$ distance method without temporal alignment in detection of Huntington's and Parkinson's diseases. The elastic functional data analysis method can provide a 94.29% accuracy for detecting Huntington's disease based on the right stance interval measurements, and 90.32% accuracy for detecting Parkinson's disease based on the right stride interval measurements. On the other hand, the $\mathbb{L}^2$ distances perform

Table 1. ALS, Huntington's and Parkinson's disease detection based on stride-to-stride gait measurements.

	PM			$\mathbb{L}^2$ distances			Center of mass
Disease	ALS	Hunt	Park	ALS	Hunt	Park	ALS
Measure	AC (%)	AC (%)	AC (%)	AC (%)	AC (%)	AC (%)	AC (%)
(1)	53.57	85.71	80.65	82.14	54.29	61.29	78.57
(2)	32.14	88.57	**90.32**	75.00	48.57	61.29	78.57
(3)	53.57	77.14	87.10	53.57	31.43	51.61	57.14
(4)	42.86	77.14	77.42	53.57	37.14	45.16	46.43
(5)	42.86	74.29	80.65	**96.43**	**65.71**	**74.19**	**92.86**
(6)	46.43	**94.29**	80.65	82.14	54.29	61.29	85.71
(7)	**60.71**	82.86	87.10	82.14	57.14	64.52	**92.86**

much better in detecting ALS (96.43% based on left stance interval) than elastic functional data analysis (60.71% based on double support interval). The ALS classification result proved to be very different from the other ones, and thus we decided to explore it further. As described in Section 2.2, one aspect of the PM is that the representation of biosignals is invariant to their vertical shifts. That is, if we add a constant to a biosignal the distance between the original and the shifted versions is zero. This is not the case when we use the $\mathbb{L}^2$ distance between them. It turns out that, in the ALS example, the two groups mainly differ through their vertical shifts. Thus, our method is rather ineffective in differentiating between them, while the $\mathbb{L}^2$ distance performs well. To support this argument, we computed the LOO-NN classification accuracy using distances based on the biosignals' centers of mass only. The center of mass of each biosignal serves as a representative of that biosignal's vertical shift. We report this result in the final column of Table 1 and note that the classification accuracies are close to the ones obtained using the $\mathbb{L}^2$ distance method.

3.2 *Detection and localization of myocardial infarction*

In this section, we present results of MI detection and localization using a subset of the PTB diagnostic database described earlier. For each subject in the data, we perform segmentation of the ECG signal into PQRST complexes using the algorithm described in Section 2.5. Furthermore, we form a signature PQRST complex for each subject using the Karcher mean. This process is repeated for each of the 15 leads provided in the data.

Detection of MI: In detection of MI, we first utilize the proposed distance measure (d) between each pair of signature PQRST complexes. We compute such distances for each lead provided in the data and perform classification using the LOO-NN classifier. In addition, we compare our result to an $\mathbb{L}^2$ distance between the signature PQRST complexes without warping (also using the LOO-NN classifier). We report the sensitivity, specificity and accuracy for each method in Table 2. We note that the PM outperforms the $\mathbb{L}^2$ distances in cases of all ECG leads. The PM can achieve a diagnostic accuracy of up to 86.88% when using leads V5 or VX. We also consider classification using combination classifiers. The results in this case are computed as follows. We

Table 2. MI detection using pair-wise distances between signature PQRST complexes.

	PM			$\mathbb{L}^2$ distances		
Classifier lead	SE (%)	SP (%)	AC (%)	SE (%)	SP (%)	AC (%)
I	71.25	86.25	78.75	58.75	56.25	57.5
II	73.75	75.00	74.38	70.00	53.75	61.88
III	72.50	91.25	81.88	55.00	67.50	61.25
aVR	77.50	90.00	83.75	63.75	63.75	63.75
aVL	77.50	92.50	85.00	52.50	65.00	58.75
aVF	61.25	88.75	75.00	61.25	58.75	60.00
V1	66.25	75.00	70.63	56.25	65.00	60.63
V2	68.75	91.25	80.00	58.75	66.25	62.50
V3	80.00	83.75	81.88	70.00	71.25	70.63
V4	76.25	83.75	80.00	68.75	62.50	65.63
V5	80.00	93.75	86.88	87.50	77.50	82.50
V6	78.75	82.50	80.63	72.50	61.25	66.88
VX	87.50	86.25	86.88	72.50	63.75	68.13
VY	70.00	83.75	76.88	55.00	60.00	57.50
VZ	78.75	81.25	80.00	66.25	57.50	61.88
Comb.	83.75	96.25	90.00	72.50	62.50	67.50

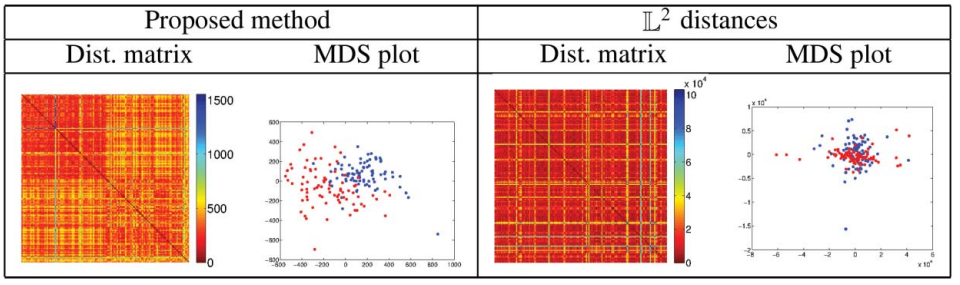

Figure 9. Distance matrices and multidimensional scaling plots for the V5 single lead classifier.

remove the test observation from the data and compute the classification accuracy of each lead based on the remaining observations. We choose the top three leads and combine their distance matrices (with equal weights). Using this combination we assign the class to the test observation using the LOO-NN method. We see that using this combination we can significantly improve the sensitivity and specificity, and we can achieve accuracy of 90%.

In Figure 9, we provide an image of the distance matrix and the multidimensional scale plot (blue: control; red: myocardial infarction) for the single lead classifier with highest detection accuracy, V5. The data displayed is organized as follows: the first 80 subjects are in the control group and the following 80 subjects are in the MI group. When using the PM to compute distances between biosignal cycles we see very nice separation (two dark blocks in the distance matrix) between the control and the MI groups. On the other hand, this separation is not clearly present for the $\mathbb{L}^2$ distance method.

The task of computing all pair-wise distances for each of the ECG leads can be computationally expensive, especially when trying to classify many subjects. Thus, an alternative classification approach is desirable, where it is possible to classify a subject using fewer distance calculations. Here, we consider such an approach by summarizing the control and MI groups using their Karcher means. We note that the ability to compute sample statistics is one of the benefits of the proposed framework, which is not the case in many of the other feature-based classification methods. This enables us, for each new subject, to compute only two distances per lead, one to the control mean and one to the MI mean. The subject is then classified using the lower of the two distances. In order to apply this classification scheme to our data, we split the total data set (160 subjects, 80 controls and 80 MIs) into a training set (80 subjects, 40 controls and 40 MIs) and a test set (80 subjects, 40 controls and 40 MIs). We compute the Karcher means for each of the groups using the training set and perform classification on the test set. For the $\mathbb{L}^2$ distance method, we compute the group means using a cross-sectional mean. The results for each of the ECG leads are reported in Table 3. We note that the performance of the PM is comparable to using all pair-wise distances. In fact, for the combination classifier (computed in the same way as described previously), the accuracy is only 1.25% lower. Again, we see that the PM outperforms using cross-sectional means and $\mathbb{L}^2$ distances without temporal alignment.

In order to validate the classification performance reported in Table 3 for the combination classifier, in Figure 10 we display each subject using their distance to the control mean as the x-coordinate and the distance to the MI mean as the y-coordinate (these are cumulative distances based on the top three single lead classifiers for each test observation). Blue subjects come from the control group and red subjects are from the MI group. We also draw the line $y = x$ to assess the separation between classes. In a perfect classification scheme, we expect all of the blue subjects to lie above this line and all of the red subjects to lie below it. For the PM, we see very little overlap between the two classes. This distinction is not nearly as clear when using $\mathbb{L}^2$ distances without warping.

Table 3. MI detection using distances to the control and MI means.

	PM			$\mathbb{L}^2$ distances		
Classifier lead	SE (%)	SP (%)	AC (%)	SE (%)	SP (%)	AC (%)
I	85.00	75.00	80.00	30.00	75.00	52.50
II	85.00	75.00	80.00	72.50	30.00	51.25
III	75.00	52.50	63.75	60.00	47.50	53.75
aVR	80.00	92.50	86.25	75.00	30.00	52.50
aVL	90.00	55.00	72.50	42.50	67.50	55.00
aVF	52.50	75.00	63.75	62.50	37.50	50.00
V1	75.00	52.50	63.75	52.50	52.50	52.50
V2	55.00	77.50	66.25	55.00	32.50	43.75
V3	57.50	100.00	78.75	67.50	80.00	73.75
V4	67.50	95.00	81.25	62.50	80.00	71.25
V5	77.50	95.00	86.25	62.50	70.00	66.25
V6	77.50	87.50	82.50	67.50	67.50	67.50
VX	80.00	92.50	86.25	80.00	65.00	72.50
VY	65.00	77.50	71.25	65.00	32.50	48.75
VZ	65.00	97.50	81.25	42.50	87.50	65.00
Comb.	82.50	95.00	88.75	82.50	87.50	85.00

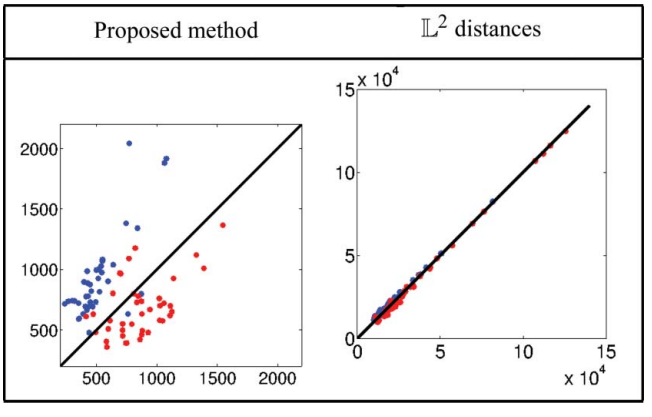

Figure 10. Classification summary for the combination classifier using distances to the means as coordinates.

Localization of MI: Next, we consider a more challenging problem of MI localization. For the purpose of this study we are concerned with only two types of MI, anterior and inferior. Out of the 80 subjects in the MI group, 77 had a type of anterior or inferior MI. We note that some of the 77 subjects had a more complicated localization of MI, for example antero-septal, but for the purpose of this classification study they were assigned to the anterior group. Table 4 shows the accuracy of LOO-NN classification using all pair-wise distances between subjects. We note that we outperform the simple $\mathbb{L}^2$ distance method in all cases. The V3 ECG lead provides the best accuracy at over 90% and the combination classifier improves this rate to over 92%.

Our classification results are consistent with standard diagnostic techniques [7,23]. In the case of anterior MI, changes in leads V2–V4 are most commonly observed. Sometimes changes can also be observed in leads aVL, V1, V5 and V6. On the other hand, in the case of inferior MI, changes in leads II, III and aVF are observed. We note that leads V2 and V3 provide the highest classification rate using the PM. In addition, leads III, aVL, aVF, V1 and V4 provide classification rates above 70%.

Table 4. Localization of MI using pair-wise distances between ECG biosignals for all ECG leads.

	PM	$\mathbb{L}^2$ distances
Classifier lead	AC (%)	AC (%)
I	59.74	58.44
II	66.23	46.75
III	71.43	51.95
aVR	54.55	50.65
aVL	70.13	46.75
aVF	74.03	48.05
V1	71.43	67.53
V2	88.31	74.03
V3	90.91	76.62
V4	76.62	74.03
V5	53.25	55.84
V6	53.25	62.34
VX	71.43	54.45
VY	66.23	61.04
VZ	77.92	61.04
Comb.	92.21	77.92

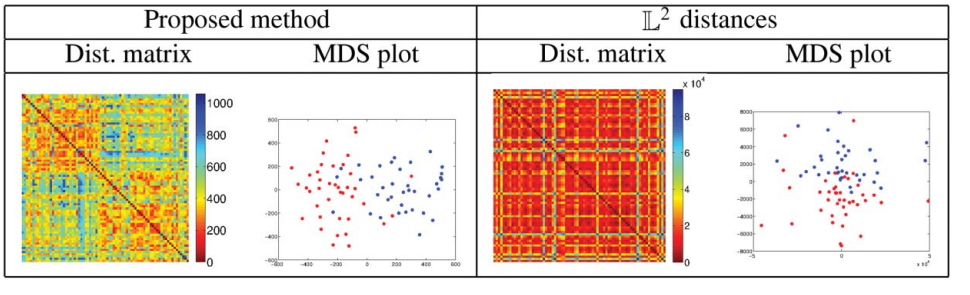

Figure 11. Distance matrices and multidimensional scaling plots for the V3 single lead classifier.

Next, in Figure 11 we display the pair-wise distance matrix and multidimensional scaling plot (blue: inferior; red: anterior) for the V3 single lead classifier, which provided best localization accuracy. In the distance matrix, the subjects are arranged in the following manner: the first 37 subjects had inferior MI followed by the 40 subjects who had anterior MI. Using the PM we can see two clear blocks corresponding to the two different types of MI. In addition, we see very nice separation of groups in the multidimensional scaling plot.

Comparison with other methods: We can compare the results obtained using the method proposed in this paper to some methods in the existing literature, which are listed in Table 5. These methods differ significantly from our method in two ways. While we utilize distances between cycles extracted from the periodic biosignal, the other works use features extracted from the raw data for classification purposes. Thus, their classification rate depends on the type of feature selected. In addition, given the extracted features, the authors train machine learning type classifiers such as artificial neural networks or random trees to obtain their final result on the testing data. In this work, we use a very simple LOO-NN classifier. Most of the methods which utilized the PTB diagnostic database reported an accuracy no better than 86%. Lahiri *et al.* [19] reported a high 96% detection rate on this data set. Arif *et al.* [2] reported a very high detection rate of 98% but their choice of training and testing data was problematic. That is, they considered classification of heart beats rather than subjects and thus heart beat data from the same subject were included in

Table 5. Comparison of the PM to other methods.

Paper	Data set	Data size	Accuracy
MI detection			
PM	PTB diag.	160 subj.	90.00%
[9]	PTB diag.	156 subj.	85.23%
[10]	PTB diag.	66 subj.	81.82%
[12]	PTB diag.	104 subj.	75.10%
[23]	Long-term ST	NA	91.62%
[19]	PTB diag.	100 subj.	96.00%
[28]	Private	116 subj.	82.80%
[21]	Private	124 subj.	SE = 96.2%, SP = 90.00%
[2]	PTB diag.	10,080 beats	98.13%
MI localization			
PM	PTB diag.	77 subj.	92.21%
[23]	PTB diag.	NA	68.57%
[21]	Private	124 subj.	SE(Ant.) = 87.5%, SE(Inf.) = 93.3%
[2]	PTB diag.	3087 beats	100.00%

both the training and testing sets, which provided skewed results. A better approach would be to use only one cycle (or a representative cycle) from each subject. With this in mind, the proposed approach to MI detection compares favorably to most of the other methods. We would also like to note that in addition to classification our method can be used for statistical modeling of biosignals, which is an important contribution. Most of the other methods reported in the current literature focused on the classification problem only and did not provide a setting for further statistical analysis such as computation of a sample mean, covariance or principal component analysis.

There is considerably less work on localization of MI. Mneimneh *et al.* [23] used a subset of the PTB diagnostic database and they reported an accuracy of approximately 69%. It is important to note though that they considered four different classes for their localization experiment while we consider only two. Arif *et al.* [2] again reported a very high accuracy for MI localization, but as stated previously their results are tainted by problematic formation of training and testing sets. Again, we note that the PM performs well in MI localization as compared with other methods.

4. Discussion

We have presented a framework for comprehensive statistical analysis of approximately periodic biosignals with application to segmentation of respiration cycles, disease classification based on stride-to-stride gait measurements, and MI detection and localization using ECG signals. This framework provides tools for automatic biosignal segmentation into cycles as well as their comparison and statistical analysis. We demonstrate the strengths of using this methodology with multiple disease classification studies. In the future, we would like to incorporate the covariance of the biosignals in our statistical models and utilize such models in a probabilistic classification scheme. Also, we would like to study the accuracy of classification obtained by combining the two distance measures d and d_ψ defined in this paper.

Acknowledgements

This research was supported in part by NSF grants DMS 0915003, IIS 1217515 and DMS 1208959. We would like to thank Dr John E. Bayouth from the Department of Radiation Oncology at the University of Iowa for providing the respiratory data.

References

[1] American Heart Association, *About Heart Attacks*, 2011. Available at http://www.heart.org/HEARTORG/Conditions/HeartAttack/AboutHeartAttacks/About-Heart-Attacks_UCM_002038_Article.jsp

[2] M. Arif, I.A. Malagore, and F.A. Afsar, *Detection and localization of myocardial infarction using k-nearest neighbor classifier*, J. Med. Syst. 36 (2012), pp. 279–289.

[3] R. Bousseljot, D. Kreiseler, and A. Schnabel, *Nutzung der EKG-Signaldatenbank CARDIODAT der PTB uber das Internet*, Biomedizinische Technik 40 (1995), pp. S317–S318.

[4] N.N. Čencov, *Statistical Decision Rules and Optimal Inferences*, Translations of Mathematical Monographs, Vol. 53, AMS, Providence, RI, 1982.

[5] G.D. Clifford, F. Azuaje, and P. McSharry, *Advanced Methods and Tools for ECG Data Analysis*, Artech House, Inc., Boston, MA, 2006.

[6] M. Derawi, P. Bours, and K. Holien, *Improved cycle detection for accelerometer based gait authentication*, Sixth International Conference on Intelligent Information Hiding and Multimedia Signal Processing, Darmstadt, Germany, 2010, pp. 312–317.

[7] H. Engblom and O. Pahlm, *ECG-MRI based localization of myocardial infarction*, in *Current News in Cardiology: Proceedings of the Mediterranean Cardiology Meeting 2007*, Taormina, Italy, May 20–22, M.M. Gulizia, ed., Springer, Milan, 2007, pp. 347–354.

[8] D. Gervini and T. Gasser, *Self-modeling warping functions*, J. R. Stat. Soc. Ser. B 66 (2004), pp. 959–971.

[9] B. Gohel and U. Tiwary, *Automated risk identification of myocardial infarction using relative frequency band coefficient (RFBC) features from ECG*, Open Biomed. Eng. J. 4 (2010), pp. 217–222.

[10] B. Gohel, U. Tiwary, and T. Lahiri, *Relative amplitude based features of characteristic ECG-peaks for identification of coronary artery disease*, First International Conference on Intelligent Human Computer Interaction, Allahabad, India, 2009, pp. 140–146.

[11] A.L. Goldberger, L.A.N. Amaral, L. Glass, J.M. Hausdorff, P.Ch. Ivanov, R.G. Mark, J.E. Mietus, G.B. Moody, C.K. Peng, and H.E. Stanley, *PhysioBank, PhysioToolkit, and PhysioNet: Components of a new research resource for complex physiologic signals*, Circulation 101 (2000), pp. e215–e220.

[12] S. Gudmundsson, T. Runarsson, and S. Sigurdsson, *Test–retest reliability and feature selection in physiological time series classification*, Comput. Meth. Program Biomed. 105 (2012), pp. 55–60.

[13] J. Hausdorff, A. Lertratanakul, M. Cudkowicz, A. Peterson, D. Kaliton, and A. Goldberger, *Dynamic markers of altered gait rhythm in amyotrophic lateral sclerosis*, J. Appl. Physiol. 88 (2000), pp. 2045–2053.

[14] J. Hausdorff, S. Mitchell, R. Firtion, C. Peng, M. Cudkowicz, J. Wei, and A. Goldberger, *Altered fractal dynamics of gait: Reduced stride-interval correlations with aging and Huntington's disease*, J. Appl. Physiol. 82 (1997), pp. 262–269.

[15] G. James, *Curve alignment by moments*, Ann. Appl. Stat. 1 (2007), pp. 480–501.

[16] A. Kneip and T. Gasser, *Statistical tools to analyze data representing a sample of curves*, Ann. Stat. 20 (1992), pp. 1266–1305.

[17] A. Kneip and J.O. Ramsay, *Combining registration and fitting for functional models*, J. Am. Stat. Assoc. 103 (2008), pp. 1155–1165.

[18] S. Kurtek, A. Srivastava, and W. Wu, *Signal estimation under random time-warpings and nonlinear signal alignment*, Neural Information Processing Systems (NIPS) Conference, Granda, Spain, 2011.

[19] T. Lahiri, U. Kumar, H. Mishra, S. Sarkar, and A. Roy, *Analysis of ECG signal by chaos principle to help automatic diagnosis of myocardial infarction*, J. Sci. Ind. Res. 68 (2009), pp. 866–870.

[20] X. Liu and H.G. Müller, *Functional convex averaging and synchronization for time-warped random curves*, J. Am. Stat. Assoc. 99 (2004), pp. 687–699.

[21] H. Lu, K. Ong, and P. Chia, *An automated ECG classification system based on a neuro-fuzzy system*, Computers in Cardiology Conference, Cambridge, MA, 2000, pp. 387–390.

[22] J. Mäntyjärvi, M. Lindholm, E. Vildjiounaite, S. Mäkelä, and H. Ailisto, *Identifying users of portable devices from gait pattern with accelerometers*, IEEE International Conference on Acoustics, Speech, and Signal Processing, Philadelphia, PA, 2005.

[23] M. Mneimneh and R. Povinelli, *An electrophysiological cardiac model with applications to ischemia detection and infarction localization*, Computers in Cardiology Conference, Park City, Utah, 2009.

[24] J.O. Ramsay and X. Li, *Curve registration*, J. R. Stat. Soc. Ser. B 60 (1998), pp. 351–363.

[25] J.O. Ramsay and B.W. Silverman, *Functional Data Analysis*, 2nd ed., Springer Series in Statistics, New York, 2005.

[26] A. Srivastava, W. Wu, S. Kurtek, E. Klassen, and J.S. Marron, *Statistical analysis and modeling of elastic functions*, ArXiv e-prints, 2011.

[27] R. Tang and H.G. Müller, *Pairwise curve synchronization for functional data*, Biometrika 95 (2008), pp. 875–889.

[28] H. Zheng, H. Wang, C. Nugent, and D. Finlay, *Supervised classification models to detect the presence of old myocardial infarction in body surface potential maps*, Computers in Cardiology Conference, Vol. 33, Valencia, Spain, 2006, pp. 265–268.